Received February 1, 2018, accepted March 11, 2018, date of publication March 13, 2018, date of current version April 4, 2018.

Digital Object Identifier 10.1109/ACCESS.2018.2815644

Two-Level Fault Detection and Isolation Algorithm for Vehicle Platoon

GAOCHAO WANG[1], YING DING[3], YANDONG HOU[1,2], YI ZHOU[1,2], (Member, IEEE), AND XIANGYI JIA[1]

[1]School of Computer and Information Engineering, Henan University, Kaifeng 475004, China
[2]International Joint Research Laboratory for Cooperative Vehicular Networks of Henan, Kaifeng 475004, China
[3]Laboratory and Equipment Management Office, Henan University, Kaifeng 475004, China

Corresponding author: Yandong Hou (hydong@henu.edu.cn)

This work was supported in part by the National Natural Science Foundation of China under Grant 61374134 and Grant 61304132 and in part by the Natural Science Foundation of Henan under Grant 162300410030.

ABSTRACT To deal with the fault of the vehicle platoon, we have established a fault detection and isolation (FDI) system with two-level fault diagnosis architecture. For simplicity, we divide the FDI architecture into two kinds: system failure and component element failure. To detect these faults, we set up the FDI mathematical model of the fleet based on the vehicular spacing, and the sensor FDI model of a certain vehicle. Meanwhile, we construct the state space model of the fleet, and design the residual generator using the space geometry method for system failure. To design the residual generation model of the fleet for component element failure, we strengthen the structure analysis of both the fleet and a certain vehicle. What's more, to elucidate the factors that cause the change of vehicle distance, the virtual force analysis is introduced. Using the adaptive threshold method, it can enhance both the sensitivity of the FDI system to the residual and the robustness to the disturbance. To promote the vehicle itself and the fleet's information perception ability, all vehicles (Autonomous Mobile Robots) are equipped with infrared distance measuring sensors, odometers, a pair of incremental optical encoders, and so on. The experimental results show that the proposed method is reliable and efficient for FDI of fleet.

INDEX TERMS FDI, fleet, structure analysis, virtual force analysis, residual generation, space geometry.

I. INTRODUCTION

With the rapid development of vehicular networking technologies, related technologies and achievements are getting from theory to reality constantly, such as vehicle-assisted reversing system, automatic parking system and unmanned vehicles, etc. As a result, the driving has become more comfortable and convenient. Unfortunately, they also bring us the traffic accident and life threatening. The Australia ''Sydney Morning Herald'' reported that about 90% of the vehicle accidents were attributed to human errors. Moreover, McCarthy believes that unmanned vehicles can help us reduce the number of vehicle accidents significantly [1]. Everything has two sides, the unmanned vehicle is not an exception, and it may bring disaster to us. The unmanned vehicle gives a priority to protect the passengers and driver, when there is taking an accident. Therefore, the loss is likely to be greater than artificial driving. The recent unmanned vehicle accident happened on September 23, 2016, and Google's unmanned car occurred a major car accident in the test. Prior to this, Pittsburgh's Uber unmanned car occurred two accidents in real-time test experiment. Tesla Model S took an accident leading the death of the driver when an autopilot was turned on, and Google's unmanned car hit a public bus in US Silicon Valley. Now the integrated control system on the vehicle becomes more and more complicated, and the requirement of control performance index gets higher and higher. If the system takes a malfunction, and cannot be eliminated in time, it will be easy to bring inconceivable loss to people's lives. Therefore, we must pay more and more attention to the safe operation of vehicle system [2].

To ensure the safety of unmanned vehicles, Monteriù *et al.* [3] took a lead in the introduction of Fault Detection and Isolation (FDI) technology to the intelligent vehicle system and an unmanned vehicle. Monteriù *et al.* [4] has succeeded in the fault detection and isolation real-time experiment with ATVR-Jr mobile robot. G. K. Fourla *et al.* [5], [6] performs fault detection and isolation for a single vehicle based on observer and residual analysis method. According to statistical data analysis, traffic accidents often occur in which the vehicle density is large, especially in the peak hours or holidays. Taking an example, there were five vehicles rear-end traffic accidents on Harbin to Dalian highway at October 6, 2016. Therefore, the problems of active safety and fault diagnosis for multi-vehicles become more and more attraction. When mentioning the multi-vehicles active safety and FDI, it's easy to think of vehicular network with the multi-vehicles collaborative control of the classic scene, which is the vehicle platoon. Furthermore, the vehicle platoon method has been studying for decades and many algorithms have been proposed, including fixed point brakes based vehicle headway [7], fleet control based lack of data [8], [9]. These algorithms are excellent for a certain vehicle. However, there are few studies on the fault diagnosis of the vehicle platoon system.

To solve such problem, in this paper, inspired by [7], [10], and [11], we aim to establish a fleet model for the fault diagnosis. As we all know, hierarchical control can make the system structure more clearly, and simplify the control model. Thus, in this model, the failure of the vehicle platoon is divided into two levels: system failure and component element failure. System failure denotes the system level of failure; and component element failure represents the specific sensor failure. For each levels, we refer to Hou's algorithm [12], [13], to isolate the failure.

It is known that model-based approach is the most popular method [14] for fault detection and isolation of the vehicle platoon. Thus, we use the model-based FDI method for the system failure. For component element failure, we use the structure analysis method to form residual formulas about sensors. In this paper, our contributions can be listed as follows: First, we deduce the residual generator of vehicular spacing according to the spatial geometry theory, and then design an adaptive threshold residual decision module to separate the fault. Second, to elucidate the factors that cause the change of vehicle distance, a method of **virtual force analysis** is introduced. Third, according to the analysis of the force of each vehicle and the kinematic formula, we get the movement trend and attitude of each smart vehicle. Forth, to reduce the external interferences and sensor errors, we apply the **adaptive threshold** to the decision-making process. Finally, **two-level fault diagnosis architecture** and isolation algorithm are verified by software simulation experiment and physical experiment with smart vehicle platoon, respectively.

The remainder of this paper is organized as follows: Section II summarizes the related works. Section III presents the model of a single vehicle, the vehicle platoon and the vehicle platoon combining with the virtual force analysis, respectively. In section IV, according to the structural analysis method and the spatial geometry theory, the residual equation of the system failure and the component element failure are given respectively, and the adaptive threshold method of the residual decision is deduced. Section V gives the corresponding relationship between faults and residuals, and shows a residual generator that is only sensitive to the j-th vehicular spacing fault by space geometry approach. The simulation results and analyses are presented in Section VI. Finally, Section VII concludes this paper.

II. RELATED WORK

Recently, the fault detection and isolation problem in cyber physical systems (CPS) has arose people immense interests from both industrial and academic communities. CPS is a system with intense interaction of entities in the physical world and the abstract information. Such systems exist in both industrial manufacturing and people's daily lives commonly. As a central investigation topic in Industrial 4.0, the concept of CPS raises vast interests in the academic world as well as in the industrial realm. Moreover, Vehicular Cyber-Physical System (VCPS) as an important part of CPS has been paid more and more attention. Qian *et al*. [15] propose a new change verification method based on the time slot occupation technique in the cluster-based Vehicular Cyber-Physical Systems, which can improve the verification efficiency significantly and obtain a high verification accuracy. Jeong and Lee [16] proposes the design of Vehicular Cyber-Physical Systems (called VCPS) for smart road services in vehicular networks. VCPS is a complex embedded network system combining computing, communications and control on the basis of environmental sensing [17], which is regarded as a high and complex systematic level. Once a fault of VCPS occurs, the consequences can be disastrous. Therefore, in this paper, we focus on the FDI of VCPS.

Monteriu *et al*. [3], [4] present experiment validation and implementation issues of a model-based sensor FDI system applied to ATVR-Jr mobile robot. In the reference [3], enhanced structural analysis is followed to build the residual generation module and the unmanned ground vehicles model. Two different methods have been proposed in [4] to detect a change in the mean of a random sequence, which includes an ''ad hoc solution'' consisting of an adaptive threshold test on the instantaneous values of the obtained residuals and a particle filtering-based likelihood ratio decision solution.

G. K. Fourlas *et al*. [5], [6] propose sensors fault diagnosis in autonomous mobile robots using observer and model based actuator fault diagnosis for a mobile robot. They use the observer-Kalman filter identification technique to provide early sensors fault diagnosis [5] and use structural analysis based technique in order to generate residuals to detect actuators faults as early as possible and provide a timely warning.

We use the model-based approach to the FDI of fleet. Y. Liu focuses on cooperative spacing control of Autonomous Vehicle with input delays, when no communication of inter-vehicles and no information of lead vehicle [11], then a virtual force approach is used to design a control strategy [7]. In [8]–[10], the model of fleet is analyzed by mathematical methods in various parameters situations. To build a vehicle platoon of fault models, with the idea of vehicle platoon modeling in [7] and [10] and the vehicle platoon mathematical modeling methods in [11], the fleet model is established based on the distance between adjacent vehicles.

The failure of the vehicle platoon is divided into two levels: system failure and component element failure. Regarding fault detection and isolation for the vehicle platoon, model-based approach is the most common method [14]. The system fault is to use the spatial geometry theory [13], [18] to design the state observer and residual generator to diagnose the vehicle platoon fault. While the residual generation and residual assessments are the main components of the model-based FDI. Moreover, component element failures are diagnosed based on the structure of the team analysis to get a series of residual formula [3], [12], [19]. In this paper, firstly, we deduce the residual generator of vehicular spacing according to the spatial geometry theory, and then design an adaptive threshold residual decision module to separate the fault [9]. The interaction between every vehicles is very complicated in the fleet [20]. To elucidate the factors that cause the change of vehicle distance, a method of virtual force analysis is introduced. According to the analysis of the force of each vehicle and the kinematic formula, we get the movement trend and attitude of each smart vehicle.

III. THE FLEET MODEL

Define the faults of fleet as two levels, namely system failure and component element failure. System failure is a system-level failure, and its parameters contain at least two cars' datum. Component element failure refers to a specific sensor failure. System failure is caused by a series of component element failures. In this paper, the system failure refers to the fault of vehicular spacing. Component element failure refers to the infrared distance measuring sensor failure (f_S), GPS failure (f_G), the right incremental optical encoder failure (f_{ER}) and the left incremental optical encoder failure (f_{EL}). Section III-A gives a single autonomous mobile robot model. The fleet model is presented in Section III-B. In Section III-C, combining with the structure analysis of the fleet, the virtual force analysis method [7] is used to model the fleet from the perspective of kinematics. Meanwhile, the failure model of the sensor in [12] and [13] is ameliorated to improve its robustness and to minimize the false alarm rate.

A. AUTONOMOUS MOBILE ROBOTS MODEL

The proposed two level fault diagnosis architecture has been implemented on a STM-32 drive autonomous mobile robot platform shown in Fig.1. And the fleet is composed of three autonomous mobile robots. We put a single autonomous mobile robot model into the coordinate system as shown in Fig.2. x is the horizontal axis, which is coincident with east direction. y is the vertical axis that is coincident with north direction. Denote the i-th vehicle's forward velocity by v_i, and θ_i is the angle between the main axis of the vehicle and the y axis. $\omega_i(t)$ represents the angular velocity of the i-th vehicle. P_i is the absolute position of the real bumper of vehicle i measured by Global Positioning System (GPS) and odometers. Then the kinematics equations are shown as follows.

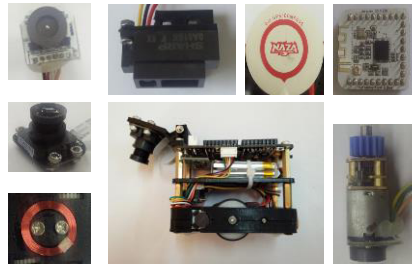

FIGURE 1. Autonomous mobile robot.

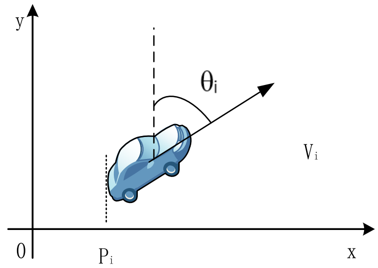

FIGURE 2. The vehicle on the XY coordinate.

$$v_i = \dot{P}_i, \tag{1}$$
$$a_i = \ddot{P}_i, \tag{2}$$
$$\dot{\theta}_i(t) = \omega_i(t), \tag{3}$$
$$\dot{x}(t) = v_i(t)\cos\theta_i(t), \tag{4}$$
$$\dot{y}(t) = v_i(t)\sin\theta_i(t). \tag{5}$$

Denote the i-th vehicle's angular velocity of the left and right wheels by ω_L^i and ω_R^i, respectively. r is the wheel radius, d is the wheelbase. Then the forward velocity and angular velocity of the i-th vehicle can be expressed by

$$v_i(t) = \frac{r}{2}(\omega_L^i(t) + \omega_R^i(t)), \tag{6}$$
$$\omega_i(t) = \frac{r}{d}(\omega_R^i(t) - \omega_L^i(t)). \tag{7}$$

We also get the latitude $\lambda_i(t)$, the longitude $\varphi_i(t)$ and the current time $T_x(t)$ of the i-th vehicle by GPS. The last set of measurement is related to the i-th vehicle variables by follows [3]:

$$\dot{x}(t) = \dot{\varphi}_i(t)R_{\varphi_0}\sin\lambda(t), \tag{8}$$
$$\dot{y}(t) = \dot{\lambda}_i(t)R_{\lambda 0}. \tag{9}$$

Moreover, the $R_{\varphi 0}$ and $R_{\lambda 0}$ are constants. And the variables of the set $\{\lambda_i\ \varphi_i\ v_i\ \omega_i\ \omega_L^i\ \omega_R^i P_i\}$ are known to vehicle i.

B. FLEET MODEL

For clarity, in Fig.3, we give the model of vehicle platoon. In addition, each follower is assigned with an index increasing in upstream direction. Here, Li represents the length of vehicle i, and the absolute position of the rear bumper of vehicle i is denoted by Pi. The time dependency will be omitted for simplicity in the following sections. v_i is the forward velocity

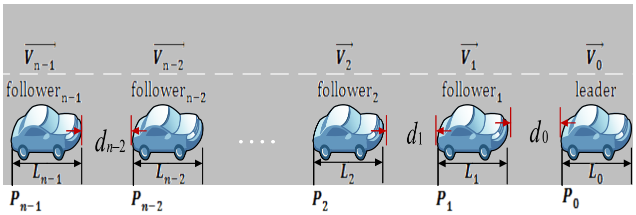

FIGURE 3. The model of vehicle platoon.

of vehicle i, and d_i is the vehicular spacing between the vehicle i and vehicle $i+1$, equals:

$$d_i = P_i - P_{i+1} - L_{k+1}, \tag{10}$$

The vehicular spacing error r_i equals:

$$r_i = d_i - d_{di}, \tag{11}$$

and d_{di} is the desired vehicular spacing of vehicle i, which will be defined via a so-called *spacing policy*.

Space policy is divided into two categories that are constant time headway (CTH) spacing policy and variable time headway (VTH) spacing policy. In this paper, we use CTH spacing policy, and the desired headway can be formulated as follows [20]:

$$d_{di} = h_{i+1}(v_{i+1}^2 - v_i^2) + t_{h_{i+1}} v_{i+1} + \Delta d_i, \tag{12}$$

where v_{i+1} and v_i are the velocity of the vehicle $i+1$ and vehicle i, respectively. h_{i+1} is a constant of vehicle $i+1$ whose size depends on the maximum deceleration performance of the vehicle. $t_{h_{i+1}}$ is the time gap which is not generally less than two seconds, and Δd_i is the minimum safe distance. Because the speed difference between the adjacent vehicles is small compared to the absolute speed relatively, the Equation (12) can be simplified as follows:

$$d_{di} = t_{h_{i+1}} v_{i+1} + \Delta d_i. \tag{13}$$

We employ the simplified vehicle model represented by [21]:

$$\begin{pmatrix} \dot{P}_i \\ \dot{v}_i \\ \dot{a}_i \end{pmatrix} = \begin{pmatrix} P'_i \\ P''_i \\ P'''_i \end{pmatrix} = \begin{pmatrix} v_i \\ a_i \\ -\tau^{-1}a_i + \tau^{-1}u_i \end{pmatrix}, \tag{14}$$

where P_i is the absolute position, v_i is the vehicle speed, a_i is the acceleration, u_i is the external input, and τ is a time constant representing the engine dynamics. Make σ be the period length. χ is the main time in every period σ. Suppose $t \in [k\sigma, k\sigma + \chi), k \in Z^+$, the P_0, v_0, a_0 of the leader are known to all followers. The control input u_0 is continuous bounded, $|u_0(t)| \leq \iota$, ι is a constant. When $t \in [k\sigma + \chi, (k+1)\sigma)$, the vehicle platoon is equilibrium state, which is zero input for each followers, using the following formation control rate:

$$\begin{cases} |u_0(t)| \leq \iota, \\ u_i(t) = g_i(v_{i+1}, v_i, v_{i-1}) \qquad t \in [k\sigma, k\sigma + \chi) \\ \qquad + f_i(P_{i+1}, P_i, P_{i-1}). \end{cases} \tag{15}$$

where $f(\cdot)$ and $g(\cdot)$ are the functions with respect to the position P_i and the velocity v_i of vehicle i, respectively.

As the inter-vehicle distances are more relevant than the absolute vehicle positions, Equation (14) can be rewritten with distance d_i as a state, instead of the position P_i, and then we get following new vehicle model [22],

$$\begin{pmatrix} \dot{d}_i \\ \dot{v}_i \\ \dot{a}_i \end{pmatrix} == \begin{pmatrix} v_{i-1} - v_i \\ a_i \\ -\tau^{-1}a_i + \tau^{-1}u_i \end{pmatrix}. \tag{16}$$

Denote the state by $\boldsymbol{x_i} = \begin{bmatrix} d_i & v_i & a_i \end{bmatrix}^T$, the equilibrium state x_{ies} of Equation (16) under the control rate Equation (15) must satisfy:

$$\boldsymbol{x_{ies}} = \begin{pmatrix} d_{ies} \\ v_{ies} \\ a_{ies} \end{pmatrix} = \begin{pmatrix} d_{es} \\ v_{es} \\ 0 \end{pmatrix}, \tag{17}$$

where d_{es} is a constant, which is more than the minimum safe distance Δd_i, and v_{es} is constant. Equation (16) can be rewritten with vehicular spacing error r_i as a state, instead of the distance d_i. According to Equation (11) to (16), we can get the following:

$$\begin{pmatrix} \dot{r}_i \\ \dot{v}_i \\ \dot{a}_i \end{pmatrix} == \begin{pmatrix} a_{i-1} - a_i - t_{h_{i+1}} a_{i+1} \\ a_i \\ -\tau^{-1}a_i + \tau^{-1}u_i \end{pmatrix}, \tag{18}$$

In summary, we employ the following class of linear invariant system with spatially invariant dynamics written in state-space form as follows [17]:

$$\dot{\boldsymbol{x}}_{\boldsymbol{i}}(t) = \sum_{j=0}^{i} \boldsymbol{A_{i-j}} \boldsymbol{x_j}(t) + \boldsymbol{B_{i-j}} \boldsymbol{u_j}(t), \tag{19}$$

$$\boldsymbol{y_i}(t) = \sum_{j=0}^{i} \boldsymbol{C_{i-j}} \boldsymbol{x_j}(t). \tag{20}$$

where the state $\boldsymbol{x_i}(t) \in \mathbb{R}^n$, $\boldsymbol{y_i}(t) \in \mathbb{R}^p$, $\boldsymbol{u_i}(t) \in \mathbb{R}^m$ denote the state, the output, and the control input vectors of the i-th vehicle subsystem, with $i \in Z$, at time $t \geq 0$, respectively. The matrix $\boldsymbol{A_{i-j}} \in \boldsymbol{R}^{n*n}$, $\boldsymbol{B_{i-j}} \in \boldsymbol{R}^{n*m}$ and $\boldsymbol{C_{i-j}} \in \boldsymbol{R}^{p*n}$ describe the influence of vehicle j on vehicle i. Note that vehicle platoon with homogeneous vehicle dynamics, constant τ in Equation (18), and constant time gap, constant $t_{h_{i+1}} = t_h$ in Equation (18), can be modeled as spatially invariant systems represented in Equation (19) and (20).

C. FLEET WITH VIRTUAL FORCE ANALYSIS MODEL

First, we make virtual force analysis for the i-th vehicle and its front vehicle $i-1$, rear vehicle $i+1$. The analysis results are shown in Fig. 4(a). Finally, to simplify the analysis model, we use three vehicles in the experimental verification. Assuming the platoon has only three vehicles, and then the force analysis is shown in Fig. 4(b). When the locomotive drives the rear carriage, each carriage of the train is subjected to the force exerted by the front and rear carriages. Referring to the force model of the train, as shown in Fig. 4(a), $F_{(i+1,i)}$ denotes the

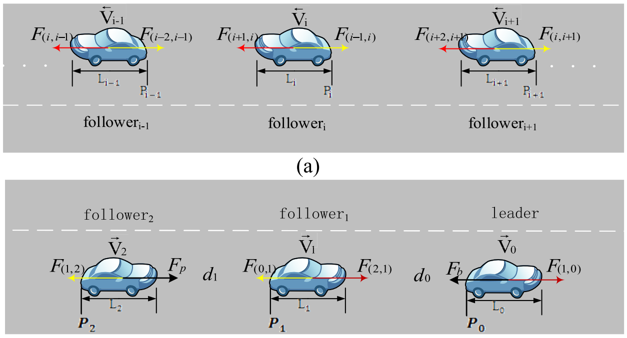

FIGURE 4. The model of fleet with virtual force.

force of follower$_{i+1}$ acting on thefollower$_i$, $F_{(i,i+1)}$ denotes the force of follower$_i$ acting on the follower$_{i+1}$. $F_{(i,i+1)}$ and $F_{(i+1,i)}$ are pairs of interaction forces, which equal in size and are in opposite directions, as shown in the following formula [7]:

$$\begin{cases} F_{(i,i-1)} = -F_{(i-1,i)} = -k_{i-1}(P_{i-1} - P_i - L_i - d_{i-1}) \\ F_{(i+1,i)} = -F_{(i,i+1)} = -k_i(P_i - P_{i+1} - L_{i+1} - d_i) \\ F_{(i+2,i+1)} = -F_{(i+1,i+2)} \\ \qquad = -k_{i+1}(P_{i+1} - P_{i+2} - L_{i+2} - d_{i+1}). \end{cases} \tag{21}$$

$k_i \in R^+ (i = 0, 1, 2 \ldots)$ is a positive constant to be designed.

Assuming the platoon has only three vehicles as shown in Fig. 4(b), we can get following formula according to Equation (21):

$$\begin{cases} F_{(1,0)} = -F_{(0,1)} = -k_0(P_0 - P_1 - L_1 - d_0) \\ F_{(2,1)} = -F_{(1,2)} = -k_1(P_1 - P_2 - L_2 - d_1), \end{cases} \tag{22}$$

where $F_{(1,0)}$ denotes the force of follower$_1$ acting on the leader, $F_{(0,1)}$ denotes the force of the leader acting on follower$_1$, $F_{(2,1)}$ denotes the force of follower$_2$ acting on *follower*$_1$, $F_{(1,2)}$ denotes the force of follower$_1$ acting on follower$_2$.

Communication between the leader and each follower is not considered as well as inter-vehicles. As a result, the control inputs are designed as Equation (15). Since the first vehicle has no foregoers, and the last vehicle has no followers, their control inputs are designed as follows:

$$\begin{cases} u_0 = g_0(v_1, v_0, v_0) + f_0(P_1, P_2, P_2 + d_{es}) \\ u_{n-1} = g_{n-1}(v_{n-1}, v_{n-1}, v_{n-2}) \\ \qquad + f_{n-1}(P_{n-1} + d_{es}, P_{n-1}, P_{n-2}), \end{cases} \tag{23}$$

Virtual force is an indirect force. For example, follower$_{i+1}$ tells follower$_i$ that it should be subjected to the magnitude and direction of the applied force, then the power system of follower$_i$ generates the virtual force $F_{(i+1,i)}$ according to the requirement itself. Besides the internal virtual forces, the braking forces F_b acting on leader is involved to make leader speed down, and the driving force F_p acting on the last vehicle of platoon is involved to make vehicle speed up. F_b and F_p are provided by the engine. $F_{(i,i+1)}$ and $F_{(i+1,i)}$ are pairs of interaction forces, which equal in size and are in opposite directions. Moreover, its size is the correlation function of the vehicular spacing. When the vehicular spacing is less than the preset safety distance, it will become larger. When the vehicular spacing is greater than the preset safety distance, it will become smaller. So taking an example, as shown in Fig. 4(b), the functions of positions f_i, $i = 0, 1, 2$ are constructed as follows:

$$\begin{cases} f_0 = F_{(1,0)} - F_b \\ f_1 = F_{(2,1)} - F_{(0,1)} \\ f_2 = F_p - F_{(1,2)}, \end{cases} \tag{24}$$

$$\begin{cases} f_1 = \alpha d_0 \\ f_2 = \alpha d_1, \end{cases} \tag{25}$$

$$v_i = v_{es}(1 + k), \tag{26}$$

$$F_p = k_{n-1} r_{n-1} + F_s, \tag{27}$$

$$F_b = k_0 O_s, \tag{28}$$

where α and k are constants. v_{es} is constant and its size is related to the minimum safe distance d_{es}. F_s and O_s are segmentation functions:

$$O_s = \begin{cases} 0, & L_0 > L_{es} \\ \rho_0(L_{es} - L_0). & otherwise \end{cases} \tag{29}$$

$$F_S = \begin{cases} \rho_{n-1}(v_{n-1} - v_{es}), & v_{n-1} \leq v_{es} \\ 0. & oherwise \end{cases} \tag{30}$$

where ρ_0 and ρ_{n-1} are constants. L_{es} is a security threshold, and L_0 is a value of the distance sensor. v_{n-1} is the velocity of last vehicle of platoon.

The function of velocity g_i, $i = 0, 1, 2$ may be set as $g_i = -k_i v_i$ [7]. Combining Equation (1), (2) with Equation (21)-(26), we obtain the dynamics of the three-vehicles platoon system as follows.

$$\begin{cases} \ddot{P}_0 = -k_0(P_0 - P_1 - L_1 - d_0) - k_0\dot{P}_0 - F_b \\ \ddot{P}_1 = -k_1(P_1 - P_2 - L_2 - d_1) \\ \qquad + k_0(P_0 - P_1 - L_1 - d_0) - k_1\dot{P}_1 \\ \ddot{P}_2 = k_1(P_1 - P_2 - L_2 - d_1) - k_2\dot{P}_2 + F_p, \end{cases} \tag{31}$$

Let us model the vehicle platoon dynamics in terms of an infinite-dimensional model with spatially invariant dynamics. Vehicle platoon with homogeneous vehicle dynamics can be modeled as spatially invariant systems represented as follows.

$$\dot{P}_i = \frac{1}{k_i}\begin{bmatrix} k_{i-1} & -k_i - k_{i-1} & k_i \end{bmatrix} \cdot \left(\begin{bmatrix} P_{i-1} \\ P_i \\ P_{i+1} \end{bmatrix} + \begin{bmatrix} -L_i - d_{i-1} \\ 0 \\ L_{i+1} + d_i \end{bmatrix} \right) - \frac{1}{k_i}\ddot{P}_i, \tag{32}$$

Denote the state by $\boldsymbol{P}(t) = \begin{bmatrix} P_0 & P_1 & P_2 & \cdots & P_{n-1} \end{bmatrix}^T$, and the output vectors $\boldsymbol{z}(t) = \begin{bmatrix} d_0 & d_1 & \cdots & d_{n-2} \end{bmatrix}^T$, the input vectors $\boldsymbol{O}(t) = \begin{bmatrix} \ddot{P}_0 & \ddot{P}_1 & \cdots & \ddot{P}_{n-1} \end{bmatrix}^T$. Combining Equation (19) (20) (23) (31) with (32), we obtain the dynamics of the n-vehicles platoon system as follows:

$$\dot{\boldsymbol{P}}(t) = \boldsymbol{A}\boldsymbol{P}(t) + \boldsymbol{B}\boldsymbol{O}(t) + \boldsymbol{A}\boldsymbol{E} \tag{33}$$

$$\boldsymbol{z}(t) = \boldsymbol{C}\boldsymbol{P}(t) + \boldsymbol{D} \tag{34}$$

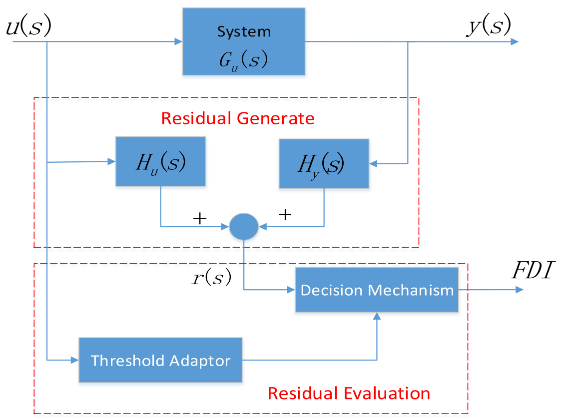

FIGURE 5. **The structure of FDI system.**

where the state $\boldsymbol{P}(\boldsymbol{t}) \in \mathbb{R}^n$, $\boldsymbol{O}(\boldsymbol{t}) \in \mathbb{R}^{n-1}$, $\boldsymbol{z}(\boldsymbol{t}) \in \mathbb{R}^m$ denote the state, the input, and the output vectors of the vehicle platoon system, respectively. The matrix $\boldsymbol{A} \in \boldsymbol{R}^{n*n}$, $\boldsymbol{B} \in \boldsymbol{R}^{n*n}$ and $\boldsymbol{C} \in \boldsymbol{R}^{(n-1)*n}$, $\boldsymbol{D} \in \boldsymbol{R}^{n-1}$, $\boldsymbol{E} \in \boldsymbol{R}^{n*n}$. Combining Equation (23) to (32), making $m_i = k_i/k_{i+1}$, and then we can get the specific parameters of system (33) and (34) as shown at the bottom of this page.

IV. RESIDUAL GENERATION AND DECISION MAKING

Hou Yandong takes the lead in using the geometric theory to solve the actuator failure, and inhibits the input interference and measurement noise effectively. To reduce the impact of sensor measurement noise on fault diagnosis, we give a residual generator of the system fault according to the method in the literature [12], [13]. The structure of FDI is shown in Fig. 5. The fault diagnosis system consists of two parts that are the residual generation unit and the residual evaluation unit.

The key to realizing fault detection and isolation is to construct a residual generator, which cannot only detect faults and but also isolate them effectively. Denote the residual signal by $\boldsymbol{r}(\boldsymbol{t})$. First, we make the residual signal $\boldsymbol{r}(\boldsymbol{t})$ compare with the adaptive threshold $TA(t)$ in the residual evaluation unit to determine whether the fault has occurred and isolated the fault simultaneously [13]. In this paper, the faults of fleet are divided into two levels. The system fault is diagnosed by using the spatial geometry theory to design the state observer and residual generator. Moreover, the component element failures are diagnosed by using the structure of the team analysis to get a series of residual formula. For the noise interference of the residual evaluation unit, we introduce the adaptive threshold.

A. RESIDUAL GENERATION OF SENSORS

We use the matching algorithm to associate the relevant variables [3], then use the known variables to replace unknown variables, and it is an equivalent replacement. Combining Equation (4) with (8), we can derive the following equation:

$$\dot{\lambda} i = \frac{v_i \sin\theta_i}{R_{\lambda 0}}, \tag{35}$$

$$\dot{\lambda}_i = \frac{d\lambda_i}{dt}, \tag{36}$$

Combining Equation (35)-(36), we have

$$r_{fG} = \frac{v_i \sin\theta_i}{R_{\lambda 0}} - \frac{d\lambda_i}{dt}. \tag{37}$$

$$\boldsymbol{A} = \begin{bmatrix} -1 & 1 & 0 & 0 & \cdots & 0 & 0 & 0 \\ m_0 & -1-m_0 & 1 & 0 & \cdots & 0 & 0 & 0 \\ 0 & m_1 & -1-m_1 & 1 & \cdots & 0 & 0 & 0 \\ \vdots & \vdots & \vdots & \vdots & \ddots & \vdots & \vdots & \vdots \\ 0 & 0 & 0 & 0 & \cdots & m_{n-3} & -1-m_{n-3} & 1 \\ 0 & 0 & 0 & 0 & \cdots & 0 & m_{n-2} & -1-m_{n-2} \end{bmatrix},$$

$$\boldsymbol{B} = \begin{bmatrix} k_0^{-1} & 0 & \cdots & 0 \\ 0 & k_1^{-1} & \cdots & 0 \\ \vdots & \vdots & \ddots & \vdots \\ 0 & 0 & \cdots & k_{n-1}^{-1} \end{bmatrix}, \quad \boldsymbol{C} = \begin{bmatrix} 1 & -1 & 0 & \cdots & 0 & 0 & 0 \\ 0 & 1 & -1 & \cdots & 0 & 0 & 0 \\ \vdots & \vdots & \vdots & \ddots & \vdots & \vdots & \vdots \\ 0 & 0 & 0 & \cdots & 1 & -1 & 0 \\ 0 & 0 & 0 & \cdots & 0 & 1 & -1 \end{bmatrix},$$

$$\boldsymbol{E} = \begin{bmatrix} 0 & -L_1-d_0 & 0 & \cdots & 0 & 0 \\ L_1+d_0 & 0 & -L_2-d_1 & \cdots & 0 & 0 \\ 0 & L_2+d_1 & 0 & \cdots & 0 & 0 \\ 0 & 0 & L_3+d_2 & \cdots & 0 & 0 \\ \vdots & \vdots & \vdots & \ddots & \vdots & \vdots \\ 0 & 0 & 0 & \cdots & -L_{n-2}-d_{n-3} & 0 \\ 0 & 0 & 0 & \cdots & 0 & -L_{n-1}1d_{n-2} \\ 0 & 0 & 0 & \cdots & L_{n-1}+d_{n-2} & 0 \end{bmatrix}$$

$$\boldsymbol{D} = \begin{bmatrix} -L_1 & -L_2 & \cdots & -L_{n-1} \end{bmatrix}^T.$$

By using the known variables to replace unknown variables, we have the following residual

$$r_{f_G} = \frac{d\lambda_i}{dt} - R_{\lambda 0}^{-1}(r\omega_R^i - \frac{d}{2}\omega_i)\sin(\arccos(\frac{d\varphi_i}{dt}\frac{2R_{\varphi 0}\cos\lambda_i}{2r\omega_R^i - d\omega_i})) \tag{38}$$

Then considering the Equation (6) and (7), rewrite them

$$r \cdot \omega_L^i = v_i - \frac{d}{2}\omega_i, \tag{39}$$

$$r \cdot \omega_R^i = v_i + \frac{d}{2}\omega_i. \tag{40}$$

Together with the above two equations, we have the following residual:

$$r_{f\,EL} = \omega_L^i - \omega_R^i + \frac{d}{r}\omega_i \tag{41}$$

Combining Equation (1) (2) (6) and (7), we can derive the following residual equation:

$$r_{f_{ER}} = \int_0^t (\ddot{P}_i - \frac{d}{dt}(r\omega_R^i - \frac{d}{2}\omega_i))dt. \tag{42}$$

Together with the Equation (16) (17) and (19), we have the last residual:

$$r_{f_s} = P_{i+1} - P_i - \int_0^t (\dot{P}_{i+1} - \dot{P}i)dt. \tag{43}$$

The vehicular spacing can be obtained in a variety of ways, such as GPS, infrared range finder, odometer, speed, the left and right wheel angular velocity. In addition, vehicular spacing may be obtained directly by a laser range finder. Other methods need to obtain data of the foregoer and itself at the same time. In the test, to reduce the interference of GPS and infrared rangefinder, we make the platoon run along the straight line.

B. RESIDUAL GENERATION OF VEHICULAR SPACING

The vehicular spacing d_i is an extremely important parameter to determine the stability and operating status of the fleet. When the vehicle is decelerating or accelerating, the vehicular spacing is adjusted within the safe range. When the fleet is stable, the vehicular spacing d_i tends to be stable, and the vehicle space is kept near the steady value d_{es}.

The size of the vehicular spacing is affected by the sensor measurement datum and other aspects. Ultimately, vehicular spacing is affected by the motor speed directly, so make the vehicle space fault of fleet as an actuator failure. Make an enactment that $\boldsymbol{L_i}$ is fault signature of the vehicle i and $\boldsymbol{m_i}$ is actuator fault model of the i-th vehicle. The subsystem (19) can be rewritten as:

$$\dot{\boldsymbol{x}}_i(t) = \sum_{j=0}^{i} \boldsymbol{A}_{i-j}\boldsymbol{x}_j(t) + \boldsymbol{B}_{i-j}\boldsymbol{u}_j(t) + \boldsymbol{L}_i\boldsymbol{m}_i(t), \tag{44}$$

Then the fault system can be given by system (33) (34) and fault subsystem (44):

$$\dot{\boldsymbol{P}}(t) = \boldsymbol{AP}(t) + \boldsymbol{BO}(t) + \boldsymbol{AE} + \sum_{i=1}^{n-1} \boldsymbol{L}_i\boldsymbol{m}_i(t), \tag{45}$$

$$\boldsymbol{z}(t) = \boldsymbol{CP}(t) + \boldsymbol{D}. \tag{46}$$

Based on the actuator fault system model (45) and (46), denote the state variable of observer by $\boldsymbol{w} \in \boldsymbol{R^n}$, the following full order observer is designed:

$$\dot{\boldsymbol{w}}(t) = \bar{\boldsymbol{A}}\boldsymbol{w}(t) - \bar{\boldsymbol{B}}\bar{z}(t) + \bar{\boldsymbol{D}}\boldsymbol{O}(t) \tag{47}$$

$$\boldsymbol{r}(t) = \bar{\boldsymbol{C}}\boldsymbol{w}(t) - \boldsymbol{G}\bar{z}(t) + \boldsymbol{MO}(t) \tag{48}$$

As can be seen from (47) and (48), requires a suitable parameter matrix $\bar{\boldsymbol{A}}$, $\bar{\boldsymbol{B}}$, $\bar{\boldsymbol{C}}$, $\bar{\boldsymbol{D}}$, $\boldsymbol{G}$ and $\boldsymbol{M}$, so that the output residual signal is not only affected by $\boldsymbol{A}$, but also satisfying from $\boldsymbol{A}$ to $\boldsymbol{B}$ is input observable. We will solve the relevant parameters, and design a residual generator that is only sensitive to the j-th vehicular spacing fault in Section IV.

C. RESIDUAL DECISION

In the system, the additive sensor failure and the mean noise of the random sequence will affect the accuracy of fault isolation. To solve this problem, the generalized likelihood ratio [23] and the critical likelihood ratio [24] method are proposed. This method can isolate the fault accurately, but the delay is large [4], so we introduce the adaptive threshold method. The size of the threshold determines the resolution of the fault isolation, so we will focus on how to select the threshold at the following.

Suppose $\Delta\boldsymbol{G_u}(s)$ is the fleet fault transfer function in the frequency domain. When there are not any faults in the system, the residual can be expressed as the following equation [14]:

$$\boldsymbol{r}(s) = \boldsymbol{H_y}(s)\Delta\boldsymbol{G_u}(s)\boldsymbol{u}(s). \tag{49}$$

Make $\Delta\boldsymbol{G_u}(s)$ be bounded, $\exists\varepsilon \in R^+$ satisfies the following formula:

$$\|\Delta\boldsymbol{G_u}(s)\| \leq \varepsilon, \tag{50}$$

Combining Equation (49) and (50), we can get

$$\|\boldsymbol{r}(s)\| \leq \varepsilon\,\|\boldsymbol{H_y}(s)\boldsymbol{u}(s)\|. \tag{51}$$

Therefore, the selection of adaptive threshold should meet the following formula:

$$TA(s) = \varepsilon\boldsymbol{H_y}(s)\boldsymbol{u}(s). \tag{52}$$

where $\boldsymbol{H_y}(s)$ is known, as long as the choice of the appropriate ε, can ensure that the fault is diagnosed effectively, while increasing the robustness to the input interference. We can obtain the approximation of ε by solving the limit of $\Delta\boldsymbol{G_u}(s)$, and then revise gradually according to the experimental results.

V. THE SPACE GEOMETRY METHOD

A. THE CORRESPONDING RELATIONSHIP BETWEEN FAULTS AND RESIDUALS

To achieve the salutation of residual generator, the corresponding relationship between faults and residuals should be discussed firstly [18].

Definition 1: Define $\boldsymbol{\Omega_i} = \{l|r_l(t) \neq 0, l = 1, 2, \cdots, p\}$ as the residual index set of i-th fault, where p represents the largest number of residuals and $\boldsymbol{m_i}(t)$ can be observed from $\boldsymbol{r_l}(t)$.

Based on the different constructions among actual systems, different residual index sets are selected. Define $\boldsymbol{\Omega_i} = \{l_1, l_2, \cdots, l_{qi}\}$, where $q_i \in \{1, 2, \cdots, p\}$. Consider the general case, it is assumed there $m \neq n$ and $\{m, n\} \in \{1, 2, \cdots, q\}$ (q is the number of fault channels). When $\boldsymbol{\Omega_m} \cap \boldsymbol{\Omega_n} = \boldsymbol{\psi}$, the m-th fault and n-th fault are independent completely, and the multiple faults can be detected completely. However, when $\boldsymbol{\Omega_m} \cap \boldsymbol{\Omega_n} \neq \boldsymbol{\psi}$, if $\boldsymbol{\Omega_m} = \boldsymbol{\Omega_n}$, the m-th fault and n-th fault are completely coupled and the multiple faults cannot be detected, else if $\boldsymbol{\Omega_m} \neq \boldsymbol{\Omega_n}$, the m-th fault and n-th fault are partly coupled and whether the multiple faults can be detected or not depends on the independent parts of fault signatures.

B. THE ALGORITHM AND STEPS OF SOLVE PARAMETER MATRICES

Firstly, we give some definitions, theorems and algorithms as follows.

Definition 2: Subspace $Im\,\boldsymbol{C} = \{y|y = \boldsymbol{C}x, x \in \Re^n\} \subseteq \Re^m$ is called image space of matrix operator $\boldsymbol{C}$, the kernel of $\boldsymbol{C}$ is the subspace

$$Ker\ \boldsymbol{C} = \{x|\boldsymbol{C}x = 0, x \in \Re^n\} \in \Re^n. \tag{53}$$

Definition 3: $\forall \boldsymbol{\Gamma} \in \Re^n$, $\hat{\boldsymbol{w}}(\boldsymbol{A}, \boldsymbol{C}, \boldsymbol{\Gamma}) = \{\boldsymbol{A}(\boldsymbol{w} \cap Ker\boldsymbol{C})) \subseteq \Re^n, \boldsymbol{\Gamma} \in \boldsymbol{w}\}$, denote all sets of $(\boldsymbol{C}, \boldsymbol{A})$ invariant subspaces containing $\boldsymbol{\Gamma}$ by $\hat{\boldsymbol{w}}(\boldsymbol{A}, \boldsymbol{C}, \boldsymbol{\Gamma})$. If $\forall \boldsymbol{w_1}$ *and* $\boldsymbol{w_2} \in \hat{\boldsymbol{w}}(\boldsymbol{\Gamma})$, have $\boldsymbol{\Gamma} \in \boldsymbol{w_1} \cap \boldsymbol{w_2}$ and $\boldsymbol{w_1} \cap \boldsymbol{w_2} \in \boldsymbol{w}(\hat{\boldsymbol{\Gamma}})$. Subspace $\boldsymbol{w}^* = inf\,\boldsymbol{w}(\boldsymbol{A}, \boldsymbol{C}, \boldsymbol{\Gamma}), \boldsymbol{\Gamma} \in \boldsymbol{w}^*$, and $\boldsymbol{w}^*$ is the minimum invariant subspace of $(\boldsymbol{C}, \boldsymbol{A})$.

Next, we will give an algorithm to compute the invariant subspace $\boldsymbol{w}^*$.

Algorithm 1 [25]: Invariant subspace $\boldsymbol{w}^*$ is solved by

$$\boldsymbol{Z_0} = \boldsymbol{\Gamma}, \tag{54}$$

$$\boldsymbol{Z_i} = \boldsymbol{\Gamma} + \boldsymbol{A}(\boldsymbol{Z_{i-1}} \cap Ker\boldsymbol{C}), (i \in \boldsymbol{k}) \tag{55}$$

where the value of $k \leq n$ is determined by condition $\boldsymbol{Z_k} = \boldsymbol{Z_{k+1}}$.

Definition 4 [26]: A subspace $\boldsymbol{S}$ is a $(\boldsymbol{C}, \boldsymbol{A})$ unobservability subspace (UOS), if $\boldsymbol{S} = \langle Ker\boldsymbol{HC}|\boldsymbol{A} + \boldsymbol{DC}\rangle$ for some measurement mixing map $\boldsymbol{H} : \Re^m \rightarrow \Re^m$ and output injection map $\boldsymbol{D} : \Re^m \rightarrow \Re^n$, where $\langle Ker\boldsymbol{C}|\boldsymbol{A}\rangle$ denotes the UOS of $(\boldsymbol{C}, \boldsymbol{A})$.

Algorithm 2: Unobservability subspace $\boldsymbol{S}^*$ is solved by

$$\boldsymbol{Z_0} = \Re^n, \tag{56}$$

$$\boldsymbol{Z_i} = \boldsymbol{w}^* + (\boldsymbol{A}^{-1}\boldsymbol{Z_{k-1}}) \cap Ker\boldsymbol{C}, (i \in k) \tag{57}$$

where the value of $k \leq n$ is determined by condition $\boldsymbol{Z_k} = \boldsymbol{Z_{k+1}}$.

Based on the concept of UOS, the next theorem provides the solvability of actuator FDI problem.

Theorem 1: Actuator faults can be detected and isolated if there exists an $(\boldsymbol{C}, \boldsymbol{A})$ UOS

$$\boldsymbol{S}_j^* = inf\,\hat{\boldsymbol{S}}(\sum_{i=1, i\neq j}^{k} \boldsymbol{\Gamma}_i), \quad (j \in k) \tag{58}$$

Such that $\boldsymbol{S}_j^* \cap \boldsymbol{\Gamma}_j = 0, i \in k$.

Proof: According to Definition 4, let $\boldsymbol{S}_j^*$ be an UOS that satisfies Equation (58), then there is a map $\boldsymbol{D}_0 \in \hat{\boldsymbol{D}}(\boldsymbol{S}_j^*)$ and $\boldsymbol{H}_j$ such that

$$\boldsymbol{S}_j^* = \langle Ker\boldsymbol{H}_j\boldsymbol{C}|\boldsymbol{A} + \boldsymbol{D}_0\boldsymbol{C}\rangle, \tag{59}$$

where $\boldsymbol{H}_j$ is a solution to

$$ker\ \boldsymbol{H}_j\boldsymbol{C} = \boldsymbol{S}_j^* + ker\boldsymbol{C}. \tag{60}$$

Let $\boldsymbol{M}_j$ be a unique solution of

$$\boldsymbol{M}_j\boldsymbol{Q}_j = \boldsymbol{H}_j\boldsymbol{C}, \tag{61}$$

$$\boldsymbol{A}_0 = (\boldsymbol{A} + \boldsymbol{D}_0\boldsymbol{C} : \Re^n/\boldsymbol{S}_j^*), \tag{62}$$

where denotes an induced map of $\boldsymbol{A}+\boldsymbol{D}_0\boldsymbol{C}$ on the factor space $\Re^n/\boldsymbol{S}_j^*$ which satisfies the following equation

$$\boldsymbol{Q}_j(\boldsymbol{A} + \boldsymbol{D}_0\boldsymbol{C}) = (\boldsymbol{A} + \boldsymbol{D}_0\boldsymbol{C} : \Re^n/\boldsymbol{S}_j^*)\boldsymbol{Q}_j. \tag{63}$$

By construction, the pair $(\bar{\boldsymbol{C}}_j, \boldsymbol{A}_0)$ is observable, hence there is a $\boldsymbol{D}_1$ such that

$$\sigma(\bar{\boldsymbol{A}}_j) = \Lambda, \tag{64}$$

where $\bar{\boldsymbol{A}}_j = \boldsymbol{A}_0 + \boldsymbol{D}_1\boldsymbol{M}_j$ and Λ is an arbitrary symmetric set. Let $\boldsymbol{D} = \boldsymbol{D}_0 + \boldsymbol{Q}_j^{-r}\boldsymbol{D}_1\boldsymbol{H}_j$, $\bar{\boldsymbol{B}}_j = \boldsymbol{Q}_j\boldsymbol{D}$, $\bar{\boldsymbol{D}}_j = \boldsymbol{Q}_j\boldsymbol{B}$, $\boldsymbol{Q}_j\boldsymbol{A} = 0$, $\boldsymbol{G}_j\boldsymbol{D} = 0$ and $\boldsymbol{M}_j = 0$.

Define $\boldsymbol{e}(t) = \boldsymbol{w}(t) - \boldsymbol{QP}(t)$. Then we have

$$\begin{aligned}
\dot{\boldsymbol{e}}_j(t) &= \dot{\boldsymbol{w}}_j(t) - \dot{\boldsymbol{Q}}_j\dot{\boldsymbol{P}}(t) \\
&= \bar{\boldsymbol{A}}_j\boldsymbol{w_j}(\boldsymbol{t}) - \bar{\boldsymbol{B}}_j(\boldsymbol{CP}(\boldsymbol{t}) + \boldsymbol{D}) + \bar{\boldsymbol{D}}_j\boldsymbol{O}(\boldsymbol{t}) \\
&\quad - \boldsymbol{Q}_j(\boldsymbol{A}_j\boldsymbol{P}(\boldsymbol{t}) + \boldsymbol{B}_j\boldsymbol{O}(\boldsymbol{t}) + \boldsymbol{A}_j\boldsymbol{E}_j + \sum_{i=1}^{k}\boldsymbol{L}_i\boldsymbol{m_i}(t)) \\
&= \bar{\boldsymbol{A}}_j\boldsymbol{w}_j(t) - \boldsymbol{Q}_j(\boldsymbol{D}_0 + \boldsymbol{Q}_j^{-r}\boldsymbol{D}_1\boldsymbol{H}_j)\boldsymbol{CP}(t) - \boldsymbol{Q}_j\boldsymbol{AP}(t) \\
&\quad - \boldsymbol{G}_j\boldsymbol{L}_j\boldsymbol{m_j}(t) \\
&= \bar{\boldsymbol{A}}_j\boldsymbol{w}_j(t) - \boldsymbol{Q}_j\boldsymbol{D}_0\boldsymbol{CP}(t) - \boldsymbol{D}_1\boldsymbol{H}_j\boldsymbol{CP}(t) - \boldsymbol{Q}_j\boldsymbol{AP}(t) \\
&\quad - \boldsymbol{G}_j\boldsymbol{L}_j\boldsymbol{m_j}(t) \\
&= \bar{\boldsymbol{A}}_j\boldsymbol{w}_j(t) - \boldsymbol{A}_0\boldsymbol{Q}_j\boldsymbol{P}(t) - \boldsymbol{D}_1\bar{\boldsymbol{C}}_j\boldsymbol{Q}_j\boldsymbol{P}(t) - \boldsymbol{Q}_j\boldsymbol{L}_j\boldsymbol{m_j}(t) \\
&= \bar{\boldsymbol{A}}_j\boldsymbol{w}_j(t) - \bar{\boldsymbol{A}}_j\boldsymbol{Q}_j\boldsymbol{P}(t) - \boldsymbol{Q}_j\boldsymbol{L}_j\boldsymbol{m_j}(t) \\
&= \bar{\boldsymbol{A}}_j\boldsymbol{e}_j(t) - \boldsymbol{Q}_j\boldsymbol{L}_j\boldsymbol{m_j}(t)
\end{aligned} \tag{65}$$

$$\begin{aligned}
\boldsymbol{r}_j(t) &= \bar{\boldsymbol{C}}_j\boldsymbol{w}_j(t) - \boldsymbol{G}_j\boldsymbol{O}(t) \\
&= \bar{\boldsymbol{C}}_j\boldsymbol{w}_j(t) - \boldsymbol{G}_j(\boldsymbol{CP}(t) + \boldsymbol{D}) \\
&= \bar{\boldsymbol{C}}_j\boldsymbol{w}_j(t) - \bar{\boldsymbol{C}}_j\boldsymbol{Q}_j\boldsymbol{P}(t) \\
&= \bar{\boldsymbol{C}}_j\boldsymbol{e}_j(t),
\end{aligned} \tag{66}$$

For the case, it is observable from $\boldsymbol{m_j}(t)$ to $\boldsymbol{r_j}(t)$, then actuator faults can be detected and isolated due to the correspondence of faults and residuals. The residual generator for the j-th actuator fault is expressed as:

$$\dot{\boldsymbol{w}}_j(\boldsymbol{t}) = \bar{\boldsymbol{A}}_j\boldsymbol{w}_j(\boldsymbol{t}) - \bar{\boldsymbol{B}}_j\bar{z}(\boldsymbol{t}) + \bar{\boldsymbol{D}}_j\boldsymbol{O}(\boldsymbol{t}) \tag{67}$$

$$\boldsymbol{r_j}(\boldsymbol{t}) = \bar{\boldsymbol{C}}_j\boldsymbol{w}(\boldsymbol{t}) - \boldsymbol{G}_j\bar{z}(\boldsymbol{t}) + \boldsymbol{M}_j\boldsymbol{O}(\boldsymbol{t}) \tag{68}$$

VI. PERFORMANCE EVALUATION

In this paper, we design the software simulation and the physical verification respectively. In the software simulation, only two vehicular spacing d_0 and d_1 of 3-vehicles platoon are monitored, as shown in Fig. 4(b). At the same time, the infrared range finder fault (f_S), left and right encoders fault (f_{EL}, f_{ER}) and the GPS fault (f_G) are monitored. In the physical verification, we use three vehicles to make up a platoon, use a roadside unit (RSU), and make the platoon go along the straight line. Take STM32 as a control unit of smart vehicle, which equips with ZigBee communication module, infrared rangefinder module, encoder speed module and other sensors. The RSU is composed of communication component ZigBee, and control component STM-32, which collects the real-time data of vehicle sensors, monitors the vehicular spacing of fleet, and uploads the data of vehicle space to host computer. When there are any vehicular spacing faults, the RSU will upload the component element failure isolated by FDI system to host computer.

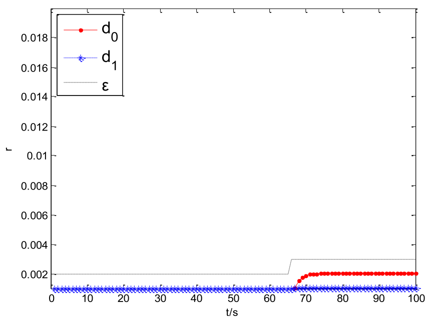

FIGURE 6. Vehicular spacing monitoring (free-fault).

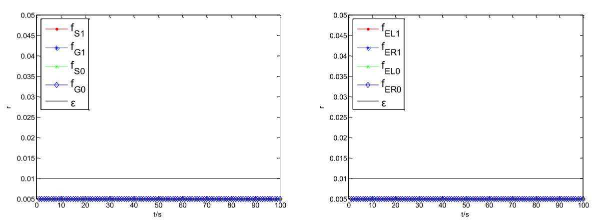

(a) (b)

FIGURE 7. The sensor FDI of d_0 (free-fault).

A. SOFTWARE SIMULATION

Fig. 6 to Fig. 13 show the software simulation results, where the simulation results are divided into two categories, which are the results of system failure and the results of component element failure. System failure is caused by component element failure. Suppose that there is a fault happening in d_0. The result of begetting the system failure is that may be a sensor failure happening in leader or follower$_1$. Fig. 6 and Fig. 9 are the effect of real-time monitoring of vehicular spacing d_0 and d_1. Moreover, the others are the results of component element failure isolated by FDI system.

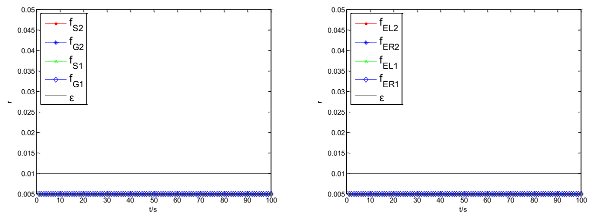

(a) (b)

FIGURE 8. The sensor FDI of d_1 (free-fault).

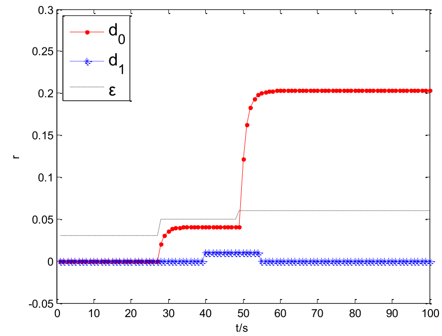

FIGURE 9. Vehicular spacing monitoring (fault).

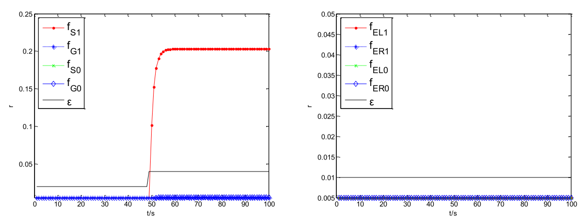

(a) (b)

FIGURE 10. The sensor FDI of d_0 (fault).

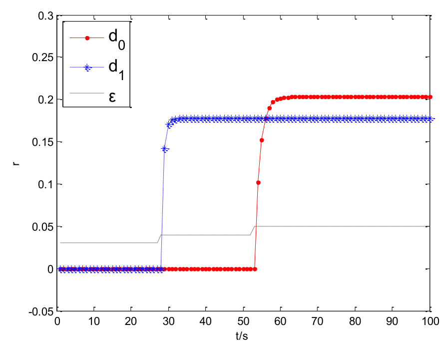

FIGURE 11. Vehicular spacing monitoring (fault).

As shown in Fig. 6, we can see that d_0 and d_1 do not exceed the set threshold, that is, the fleet is running normally. We can see that there is not any sensor failure occurring in vehicle platoon from Fig. 7 and Fig. 8 as well. From Fig. 6, we can see that d_0 is disturbed in about 67s, and the adaptive threshold has made a reasonable adjustment to stop the fault of false positives effectively.

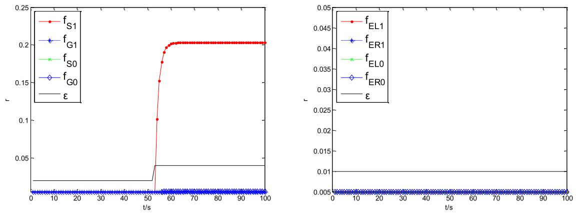

(a) (b)

FIGURE 12. The sensor FDI of d_0 (f_{S1}).

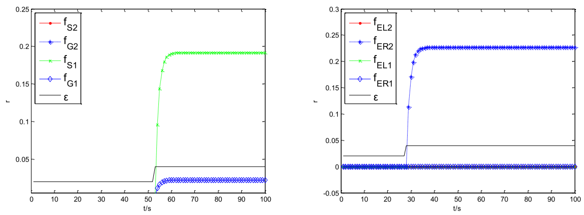

(a) (b)

FIGURE 13. The sensor FDI of d_1 (f_{S1} and f_{ER1}).

Fig. 9 and Fig. 10 show the results of the system failure and component element failure. We can see that there is a vehicle space fault about d_0 and the vehicle space d_1 is running smoothly from Fig. 9. Whether it is the sensor failure of leader, or the sensor failure of follower$_1$, will cause the failure of vehicle space d_0. Fig. 10 shows which vehicle has occurred the failure and what failure has happened. As can be seen from Fig. 10 clearly, the infrared rangefinder sensor has occurred a failure, causing a failure of vehicle space d_0.

Fig. 9 and Fig. 10 show the fault simulation results of vehicular spacing d_0, which only a certain sensor happening failure causes a system failure. It can be seen from Fig. 11 that the vehicle space d_0 has a failure when about t = 28s, and the vehicle space d_1 has a failure when about t = 53s, respectively. There are happening an infrared distance sensor failure of follower$_1$ and a failure of the right speed sensor of follower$_2$, as shown in Fig. 12 and Fig. 13.

B. PHYSICAL VERIFICATION

The algorithm and fault architecture proposed in this paper are verified by fleet of three intelligent vehicles. At first, three smart cars forming a fleet run along the straight line, and the vehicular spacing is kept within the preset controllable range, as shown in Fig. 14(a). There is a RSU locating near the fleet. The intelligent vehicle perceives itself information and the surrounding environment information, which is sent to the RSU after a simple processing in the test. The RSU processes the data, and then uploads the results to the host computer.

Fig. 14 shows the verification scenes. At the beginning, the fleet is running steadily, as shown in Fig. 14(a), and the results displayed on the host computer are correspond to the scenes shown in Fig. 15(a). The distance between follower1 and the leader is larger significantly, as shown in Fig. 14(b).

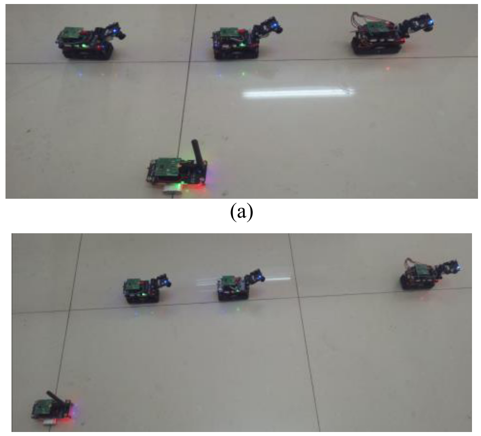

(b)

FIGURE 14. Physical verification. (a) Driving normally. (b) Fault scene.

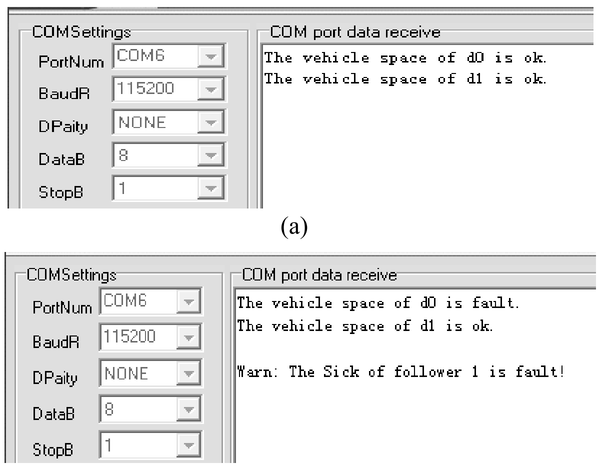

(b)

FIGURE 15. The results of Physical verification. (a) Driving normally. (b) Fault scene.

At this time, the host computer gives a warning, and isolates a specific failure, as shown in Fig. 15(b).

VII. CONCLUSION AND FUTURE WORK

In this paper, we propose a two-level fault detection and isolation algorithm for fleet. To deal with the fault of fleet, the vehicle platoon is modeled and analyzed based on the theory of spatial geometry and structural analysis. We define the fleet faults as two levels, namely, system failure and component element failure. To cope with the sensor error and external interference, the adaptive threshold method is adopted to evaluate the residual. The experimental results show that the proposed method can make a simple and effective fault detection and isolation for the fleet. However, the FDI architecture has some shortcomings because we only consider the stable driving fleet named the steady car-following fleet. For the others state of the fleet, it will cause a significant change in vehicular spacing, which in this article will be treated as a fault. Therefore, in the future, we will improve the algorithm to adopt to more traffic scenes, and transplant the algorithm proposed in this paper to the real vehicles.

REFERENCES

[1] W. Shan. (Oct. 10, 2016). Confront the unmanned car ethic and the reality of the conflict. China Quality News. [Online]. Available: http://epaper.cqn.com.cn/html/2016-10/24/content_73671.htm?div=-1

[2] Z. Donghua and Y. Yinzhong, *Modern Fault Diagnosis and Fault Tolerant Control*. Beijing, China: Tsinghua Univ. Press, 2000.

[3] A. Monteriu, P. Asthana, K. Valavanis, and S. Longhi, ''Experimental validation of a real-time model-based sensor fault detection and isolation system for unmanned ground vehicles,'' in *Proc. 14th Medit. Conf. Control Autom.*, 2006, pp. 1–8.

[4] A. Monteriu, P. Asthan, K. Valavanis, and A. Longhi, ''Model-based sensor fault detection and isolation system for unmanned ground vehicles: Experimental validation (part II),'' in *Proc. IEEE Int. Conf. Robot. Autom.*, Apr. 2007, pp. 2744–2751.

[5] G. K. Fourlas, G. C. Karras, and K. J. Kyriakopoulos, ''Sensors fault diagnosis in autonomous mobile robots using observer—Based technique,'' in *Proc. Int. Conf. Control, Autom. Robot.*, Singapore, 2015, pp. 49–54.

[6] G. K. Fourlas, S. Karkanis, G. C. Karras, and K. J. Kyriakopoulos, ''Model based actuator fault diagnosis for a mobile robot,'' in *Proc. IEEE Int. Conf. Ind. Technol. (ICIT)*, Mar. 2014, pp. 79–84.

[7] Y. Liu, B. Xu, and H. Gao, ''Cooperative braking control for a platoon of vehicles under constraint with target stopping positions,'' in *Proc. 35th Chin. Control Conf. (CCC)*, 2016, pp. 9282–9287.

[8] R. Merzouki, B. Conrard, P. Kumar, and V. Coelen, ''Model based tracking control using Jerky behavior in platoon of vehicles,'' in *Proc. Eur. Control Conf. (ECC)*, 2013, pp. 3488–3493.

[9] T.-N. Manh, M.-P. Xuan, P.-N. Doan, and T.-P. Quoc, ''Tracking control for mobile robots with uncertain parameters based on model reference adaptive control,'' in *Proc. Int. Conf. Control, Autom. Inf. Sci. (ICCAIS)*, 2013, pp. 18–23.

[10] W. Yue, L. Wang, and G. Guo, ''Event-triggered platoon control of vehicles with time-varying delay and probabilistic faults,'' *Mech. Syst. Signal Process.*, vol. 87, pp. 96–117, Mar. 2017.

[11] Y. Liu and C. Pan, ''Cooperative spacing control for autonomous vehicle platoon with input delays,'' in *Proc. Chin. Control Decision Conf. (CCDC)*, 2016, pp. 6238–6243.

[12] Y. Hou, Z. Chen, and T. Tang, ''Multi-sensor fault detection and isolation algorithm,'' *CIESC J.*, vol. 61, no. 8, pp. 2008–2014, 2010.

[13] Y. Hou, C. Wen, and Z. Chen, ''Designing method of residual generator for multi-sensor fault detection and isolation,'' *CTA Electron. Sinica*, vol. 39, no. 2, pp. 429–434, 2011.

[14] R. J. Patton and J. Chen, ''Advances in fault diagnosis using analytical redundancy,'' in *Proc. IEE Colloq. Plant Optim. Profit*, London, U.K., 1993, p. 612.

[15] J. Qian, T. Jing, Y. Huo, H. Li, and Z. Li, ''Efficient change verification of member cardinality in cluster-based VCPS,'' in *Proc. Int. Conf. Identificat., Inf., Knowl. Internet Things (IIKI)*, Beijing, China, 2015, pp. 169–174.

[16] J. Jeong and E. Lee, ''VCPS: Vehicular Cyber-physical Systems for Smart Road Services,'' in *Proc. 28th Int. Conf. Adv. Inf. Netw. Appl. Workshops*, Victoria, BC, Canada, 2014, pp. 133–138.

[17] P. Garraghan, D. McKee, X. Ouyang, D. Webster, and J. Xu, ''SEED: A scalable approach for cyber-physical system simulation,'' *IEEE Trans. Serv. Comput.*, vol. 9, no. 2, pp. 199–212, Mar./Apr. 2016.

[18] Y. Hou, Y. Jin, and Q. Cheng, ''Based on space geometry method for actuator fault detection and isolation with disturbances and noises,'' in *Proc. 33th Chin. Control Conf. Nanjing*, 2014, pp. 3164–3168.

[19] G. Wang *et al.*, ''Model-based sensor fault detection and isolation for vehicles platoon,'' *J. Shandong Univ. Sci., Technol.*, vol. 36, no. 4, pp. 51–59, Aug. 2017.

[20] P. Wang, ''An improved cooperative adaptive cruise control (CACC) algorithm considering invalid communication,'' *Chin. J. Mech. Eng.*, vol. 27, no. 3, pp. 468–474, 2014.

[21] S. S. Stankovic, M. J. Stanojevic, and D. D. Siljak, ''Decentralized overlapping control of a platoon of vehicles,'' *IEEE Trans. Control Syst. Technol.*, vol. 8, no. 5, pp. 816–832, Sep. 2000.

[22] A. Firooznia, J. Ploeg, N. van de Wouw, and H. Zwart, ''Co-design of controller and communication topology for vehicular platooning,'' *IEEE Trans. Intell. Transp. Syst.*, vol. 18, no. 10, pp. 2728–2739, Oct. 2017.

[23] B. M. E. Basseville, M. Basseville, and I. V. Nikiforow, *Election of Abrupt Changes: Theory and Application* (Information & System Sciences Series). Englewood Cliffs, NJ, USA: Prentice-Hall, 1993, pp. 326–327.

[24] F. Gustafsson, ''The marginalized likelihood ratio test for detecting abrupt changes,'' *IEEE Trans. Autom. Control*, vol. 41, no. 1, pp. 66–78, Jan. 1996.

[25] M. A. Massoumnia, *A Geometric Approach to Failure Detection and Identification in Linear Systems*. Cambridge, MA, USA: Massachusetts Inst. Technol., 1986.

[26] M.-A. Massoumnia, ''A geometric approach to the synthesis of failure detection filters,'' *IEEE Trans. Autom. Control*, vol. AC-31, no. 9, pp. 839–846, Sep. 1986.

GAOCHAO WANG received the B.E. degree from Minsheng College, Henan University, Kaifeng, China, in 2015. He is currently pursuing the M.E. degree with the School of Computer and Information Engineering, Henan University. His research interests include fault diagnosis, intelligent collaborative intersections, and Internet of Vehicles.

YING DING was born in Henan, China, in 1965. He is currently a Senior Engineer with the Henan University, Kaifeng, Henan, where he is also a Deputy Director with the Office of Laboratory and Equipment.

YANDONG HOU received the B.S. degree in electronic engineering from the China University of Mining and Technology, China, in 1996, and the Ph.D. degree in power electronics and power transmission from Shanghai Maritime University, Shanghai, China, in 2010. He is currently a Professor with the School of Computer and Information Engineering, Henan University, Kaifeng, Henan. His research interests include fault diagnosis and safety prediction in complex systems.

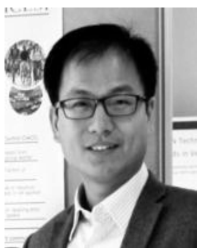

YI ZHOU (M'15) received the B.S. degree in electronic engineering from the First Aeronautic Institute of Air Force, China, in 2002, and the Ph.D. degree in control system and theory from Tongji University, China, in 2011. From 2002 to 2005, he was a Research and Development Engineer with Beijing Centergate Technologies Co, Ltd., China. He was a Visiting Researcher with the Telecommunications Research Center (ftw.), Vienna, Austria, in 2009, and the National Institute of Informatics, Tokyo, Japan, in 2010. From 2014 to 2015, he was a Post-Doctoral Fellow with the University of Waterloo, Waterloo, ON, Canada. He is currently an Associate Professor with the School of Computer and Information Engineering, Henan University, Kaifeng, China. He is the Director of the International Joint Research Laboratory for Cooperative Vehicular Networks, Henan, China. He also leads the Vehicular Networking Institute of Central Plains Silicon Valley. His research interests include vehicular cyber-physical systems and multi-agent design for vehicular networks. He is a member of the Institute of Electronics, Information, and Communication Engineers.

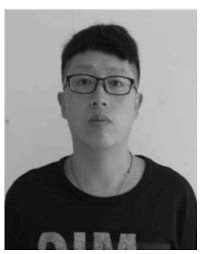

XIANGYI JIA received the B.E. degree from Minsheng College, Henan University, Kaifeng, China, in 2016. He is currently pursuing the M.E. degree with the School of Computer and Information Engineering, Henan University. His research interests include fault diagnosis.